A Robust Solution of Integrated SITAN with TERCOM Algorithm: Weight-Reducing Iteration Technique for Underwater Vehicles' Gravity-Aided Inertial Navigation System

Article *in* Navigation - Journal of The Institute of Navigation · April 2017

DOI: 10.1002/navi.176

CITATIONS
39

READS
257

7 authors, including:

Erhu Wei
Wuhan University
123 PUBLICATIONS **387** CITATIONS
SEE PROFILE

Cuijun Dong
Wuhan University
5 PUBLICATIONS **49** CITATIONS
SEE PROFILE

Liu Jiandong
Laboratoire de Météorologie Dynamique, French National Centre for Scientific Resea…
22 PUBLICATIONS **118** CITATIONS
SEE PROFILE

Tang Shenquan
Wuhan University
3 PUBLICATIONS **39** CITATIONS
SEE PROFILE

A Robust Solution of Integrated SITAN with TERCOM Algorithm: Weight-Reducing Iteration Technique for Underwater Vehicles' Gravity-Aided Inertial Navigation System

ERHU WEI, CUIJUN DONG, YALI YANG, and SHENQUAN TANG
School of Geodesy and Geomatics, Wuhan University, Wuhan, China

JIANDONG LIU
Shanghai Astronomical Observatory, Chinese Academy of Sciences, Shanghai 200030, China

GUANGYU GONG
Army of Chinese People's Liberation, Urumchi, China

ZHIHONG DENG
Beijing Institute of Technology, Beijing, China

Received December 2015; Revised August 2016

ABSTRACT: *The robustness of the Sandia Inertial Terrain-Aided Navigation (SITAN) algorithm has a pivotal influence on underwater vehicles' Gravity-Aided Inertial Navigation Systems (GAINS). An abrupt glitch of the accuracy of the GAINS will evolve into a disaster when vehicles pass through areas of smooth gravity. In order to resolve vulnerability issues of initial error and linearization error, we propose the Correlation SITAN algorithm with Weight-Reducing Iteration Technique (CSITAN + WRIT), in which the correlation process equals Terrain Contour Matching (TERCOM). The CSITAN algorithm is a Multipoint-based Extended Kalman Filtering (MEKF) method, which can work in real time. First, we need to derive the state equation and observation equation of the Multipoint-based SITAN algorithm based on the principle of the traditional SITAN algorithm. Then the accuracy of the state prediction can be improved, and the linearization error can be reduced by the correlation method based on TERCOM. Finally, the WRIT is utilized to reduce the possible influence of gross errors existing in the results of the MEKF and to extract a value with higher precision. The experimental results show that CSITAN + WRIT can achieve better accuracy and higher success rate of matching and can improve the possibilities of the occurrence of large matching errors than traditional SITAN methods in areas with smooth gravity.*

INTRODUCTION

The Gravity-Aided Inertial Navigation System (GAINS) is being widely used in underwater vehicles to bind the inherent errors of Inertial Navigation Systems (INS) that accumulate over time and could even lead to divergence of the vehicles' position [1]. The vehicles' state is updated by comparing the measurements of gravity information acquired by the gravity sensor and the values extracted from the gravity reference map based on INS information [2–5]. The structure of GAINS is shown in Figure 1.

The matching algorithms of GAINS have a high impact on the accuracy and efficiency of localization; those commonly used matching algorithms include Terrain Contour Matching (TERCOM) algorithm, iterated closest contour point (ICCP) algorithm, Sandia Inertial Terrain-Aided Navigation (SITAN), and so forth. TERCOM and ICCP are both maximum correlation and extremum judgment-based matching algorithms, which have the shortcoming of weak real-time performance. SITAN is a Kalman filtering (KF)-based matching algorithm, which has the ability to work in real time but is vulnerable to initial error and linearization error and could easily become diverged or mismatched [6].

In order to resolve these problems, [7] proposed an AFTI/SITAN algorithm that can determine the position of aircraft within a 926-m (0.5 nmi) CEP circle and estimate its position continuously at the

NAVIGATION: *Journal of The Institute of Navigation*
Vol. 64, No. 1, Spring 2017
Printed in the U.S.A.

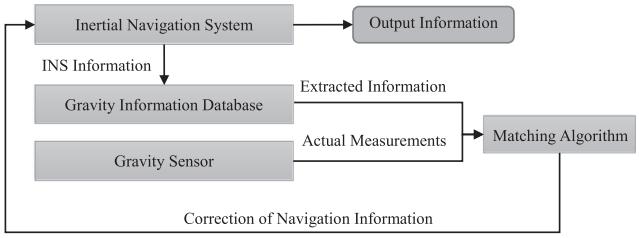

Fig. 1–The structure chart of GAINS. [Color figure can be viewed at wileyonlinelibrary.com and www.ion.org]

frequency of 3 Hz. By using cartographic-based digital terrain elevation data, it can achieve a median accuracy of less than 100 m under the conditions of gently rolling, forested terrain. [8] proposed a HELI/SITAN algorithm that utilizes a set of single-state Kalman filters to obtain favorable accuracy of positions even under large initial errors and position median radial error of real-time implementation less than 50 m. [9] proposed a Triangle Matching Algorithm, which contains the initial matching stage and the tracking matching stage that can work under a wide range of initial errors, from 0.05 deg to 0.002 deg. [10] realized the TAN system by particle filter and Gaussian mixture filter in a Bayesian framework that obeyed the principle of achieving the optimal properties with limited resource. [11] utilized a Sigma-Point Filter for Terrain Referenced Navigation, which showcased higher performance and higher robustness in terrain referenced navigation systems. [12] introduced the marginalized particle filter (MPF) to solve the nonlinear problem of the TAN system and achieved suboptimal precision by approximation to the Cramer–Rao lower bound. [13] proposed an improved TERCOM-aided INS algorithm that can correct the velocity error of INS by using a linear Kalman Filter.

In this paper, we intend to improve robustness and matching accuracy with a simple and existing method; thus, the Correlation SITAN algorithm with Weight-Reducing Iteration Technique (CSITAN + WRIT) is proposed to improve the robustness of SITAN while maintaining its advantage of good real-time performance. CSITAN is actually an organic integration of multiple applicable methods, including Multipoint-based Extended Kalman Filtering (MEKF), Correlation, and the WRIT. The algorithm is divided into three steps: the first step is to derive the state equation and observation equation of the Multipoint-based SITAN algorithm based on the principle of the traditional SITAN algorithm; the second step is to integrate the correlation method into MEKF to improve the reliability and accuracy of the state prediction. Finally, the weight-reducing iteration technique is utilized to reduce the possible influence of gross errors existing in the results of the MEKF and to extract a value with higher precision. Experimental results have verified the feasibility and robustness of CSITAN + WRIT.

The principle of the traditional SITAN algorithm and CSITAN + WRIT is introduced in Section 2 in detail. In Section 3, three trajectories with different roughness of gravity anomaly are selected to implement experiments to verify the feasibility and robustness of CSITAN + WRIT. The analyses of the results of the experiments are also given. Finally, conclusions and further discussions are provided based on the experimental results.

PRINCIPLE OF THE TRADITIONAL SITAN ALGORITHM AND CSITAN + WRIT

Principle of SITAN

The SITAN is an Extended Kalman Filter (EKF)-based matching algorithm, which utilizes the recursive optimal estimation method to update the states of underwater vehicles [14, 15]. The construction of the state equation and observation equation of SITAN is as follows.

(1) The State Equation

In this paper, six variables were selected to establish the state vector, which are as follows:

$$X_{k-1} = \left[\lambda_{k-1} \;\; \varphi_{k-1} \;\; V_{\lambda_{k-1}} \;\; V_{\varphi_{k-1}} \;\; a_{\lambda_{k-1}} \;\; a_{\varphi_{k-1}}\right]^T_{6\times 1}$$

The six variables represent the position, velocity, and acceleration in direction of longitude and latitude, respectively [16]. Thus, the state transition matrix and system noise matrix shall be established according to the state vector.

The state transition matrix $\Phi_{k|k-1}$ and the system noise matrix w_{k-1} are as follows:

$$\Phi_{k|k-1} = \begin{bmatrix} 1 & 0 & T & 0 & T^2/2 & 0 \\ 0 & 1 & 0 & T & 0 & T^2/2 \\ 0 & 0 & 1 & 0 & T & 0 \\ 0 & 0 & 0 & 1 & 0 & T \\ 0 & 0 & 0 & 0 & 1 & 0 \\ 0 & 0 & 0 & 0 & 0 & 1 \end{bmatrix}_{6\times 6},$$

$$w_{k-1} = \begin{bmatrix} w_\lambda \\ w_\varphi \\ w_{v\lambda} \\ w_{v\varphi} \\ w_{a\lambda} \\ w_{a\varphi} \end{bmatrix}_{6\times 1}$$

(2) The Observation Equation

The difference between the actual measurement of the gravity anomaly and the value extracted from

the gravity anomaly map with INS information is regarded as the observation value [17, 18].

The actual measurement of the gravity anomaly:

$$g_m = g_r(\lambda, \varphi) + \gamma_r \tag{7}$$

In Equation (7), g_m represents the measurement of the gravity anomaly, λ, φ is the true position of vehicles, $g_r(\lambda, \varphi)$ is the true value of the gravity anomaly that corresponds to true position, and γ_r is the measurement noise.

The value being extracted from the gravity anomaly map with INS information is

$$g_e = g_e(\lambda_{ins}, \varphi_{ins}) = g_r(\lambda + \delta\lambda, \varphi + \delta\varphi) + \gamma_m \tag{8}$$

In formula (8), g_e represents the extracted value of the gravity anomaly map, δx and δy are the errors in the vehicle's position, $g_r(x + \delta x, y + \delta y)$ is the true value of the gravity anomaly that corresponds to the position assigned by INS, and γ_m is the noise of measurement and quantization in digital map making.

Then the observation equation of SITAN can be obtained in the following derivation process:

$$\begin{aligned} Z &= g_m - g_e = g_r(\lambda, \varphi) + \gamma_r - g_e(\lambda + \delta\lambda, \varphi + \delta\varphi) \\ &= g_r(\lambda, \varphi) + \gamma_r - g_r(\lambda + \delta\lambda, \varphi + \delta\varphi) - \gamma_m \\ &= g_r(\lambda, \varphi) + \gamma_r - g_r(\lambda, \varphi) - \frac{\partial g_e(\lambda, \varphi)}{\partial \lambda}\delta\lambda \\ &\quad - \frac{\partial g_e(\lambda, \varphi)}{\partial \varphi}\delta\varphi - \gamma_m - \gamma_l \\ &= -h_\lambda \delta\lambda - h_\varphi \delta\varphi + \gamma_r - \gamma_m - \gamma_l \end{aligned} \tag{9}$$

The first-order Taylor series expansion method is utilized in the above process to simplify the observation equation into a linearized equation, and γ_l represents the linearization error. The final simplified observation equation is obtained in the following form:

$$Z_k = H_k X_k + V(k) \tag{10}$$

In formula (10), $V(k) = \gamma_m - \gamma_r - \gamma_l$ represents the error terms, and the coefficient matrix is shown as follows:

$$H_k = \left[-h_\lambda, -h_\varphi, -h_\lambda(k-1)\cdot T, -h_\varphi(k-1)\cdot T, \frac{-h_\lambda(k-1)T^2}{2}, \frac{-h_\varphi(k-1)T^2}{2} \right]_{1\times 6}$$

$-h_\lambda(k-1)$, $-h_\varphi(k-1)$ represent the slopes of the waypoint in $(k-1)$-th moment in the directions of east and north, and we derive the coefficient matrix based on the motion equation because $\delta\lambda, \delta\varphi$ is related to velocity and acceleration [19].

The coefficients of the observation equation are obtained by utilizing the nine-point fitting method to linearize the local background field. Its principle is introduced in the following section.

The Nine-Point Fitting Method

There are three commonly used linearization methods, including the first-order Taylor expansion method, nine-point fitting method, and whole plane fitting method. While the first one requires less time with low precision, the last one has high precision but is time-consuming [20]. Thus, we choose the nine-point fitting method to linearize the local background field. The analytical model is shown in Figure 2.

The interval between two adjacent points is $1.5\delta_\varphi$ or $1.5\delta_\lambda$ in the direction of latitude or longitude, respectively. Then calculate the correlated parameters with P_5 taken as the center point of the fitting region. The calculation formulas are shown as follows:

$$\begin{cases} g = \dfrac{1}{9}\sum_{i=1}^{9} g(k_{ix}, k_{iy}) \\ h_x = \dfrac{g_3 + g_6 + g_9 - (g_1 + g_4 + g_7)}{6Md} \\ h_y = \dfrac{g_7 + g_8 + g_9 - (g_1 + g_2 + g_3)}{6Nd} \end{cases}$$

In this formula, $g_1, g_2 \ldots g_9$ is the gravity anomaly at nine points, $M = 1.5\delta_\lambda$, $N = 1.5\delta_\varphi$.

The Principle of CSITAN + WRIT

The Procedure of CSITAN + WRIT

CSITAN + WRIT is actually a multipoint-based recursive optimal estimation method, which has the advantage of working in real time. It is divided into three steps. The first step is to derive the state equation and observation equation of the multipoint-based SITAN algorithm based on the principle of the traditional SITAN algorithm. The

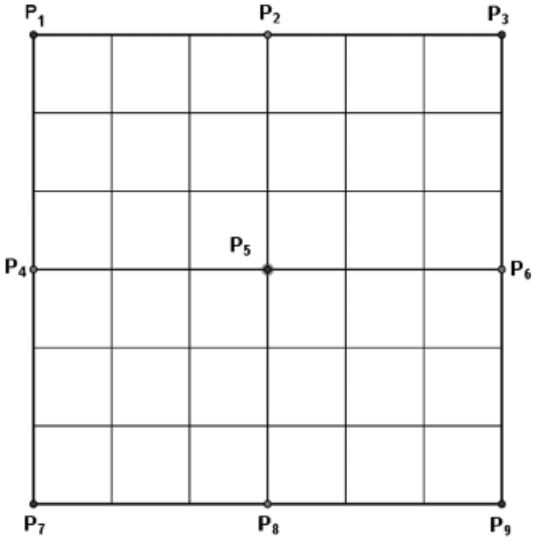

Fig. 2–Nine-point fitting method. [Color figure can be viewed at wileyonlinelibrary.com and www.ion.org]

second step is to integrate the correlation method into MEKF to improve the reliability and accuracy of the state prediction. Finally, the weight-reducing iteration technique is utilized to reduce the possible influence of gross errors existing in the results of the MEKF and to extract a value with higher precision. The flow chart of CSITAN + WRIT is shown in Figure 3:

$X'_{(k \mid k-1)}$, represents the states being processed by correlation function; $X'_{(k \mid k)}$, represents the states being corrected by actual measurements; Δ represents the differences between the predicted states and the states being processed by correlation function; and τ is the threshold value.

The procedure of CSITAN + WRIT can be briefly described as follows:

Step I: Predict the state of point sequence of the next moment based on the current state of point sequence.

Step II: Utilize the multipoint correlation method to renew the predicted states of point sequence. This step is taken under the assumption that an inaccurate state equation could bring a large deviation to the state prediction, just like there are large gross errors that exist. If this happens, the state prediction would greatly deviate from the real positions, which theoretically exist. The potential gross errors can be eliminated after the correlation process to make it closer to the real positions that exist. Because the coefficients of the observation equation were obtained through the linearization of local gravity background, a more accurate state prediction of position brings more accurate linearized coefficients.

Step III: Check the differences between the states of point sequence before and after the correlation process. Accept the processed states if the differences exceed the threshold. Because there will be a significant correction to the state prediction after the correlation process if gross errors do exist, the threshold value

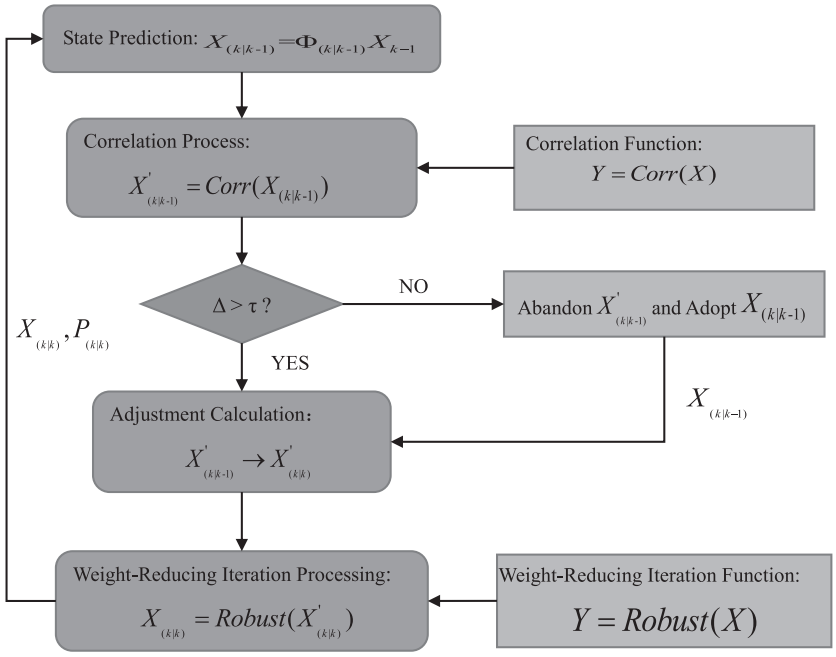

Fig. 3–The flow chart of CSITAN + WRIT. [Color figure can be viewed at wileyonlinelibrary.com and www.ion.org]

is two times the largest mean square error of positions in the state prediction.

Step IV: Correct the states of point sequence with actual measured gravity anomalies and store each of the results for each point.

Step V: Utilize the weight-reducing iteration technique to reduce the possible influence of gross errors and extract a final result for each point position. All the waypoints, except a few at the beginning and the end of the trajectory, will be processed for n times in the course of recursion. Thus, we can use the duplicate position information of one point to extract a value with higher precision.

Some technical details in CSITAN + WRIT will be introduced later in this section.

The Establishment of State Equation and Observation Equation

The establishment of the state equation and observation equation of CSITAN + WRIT has the same principle as that of the traditional SITAN algorithm except that it is a multipoint-based Recursive Optimal Estimation [9, 21].

(1) The Establishment of State Equation

We select the positions of 10 waypoints, plus the velocities and accelerations of the last point in the point sequence to establish the state vector, which are as follows:

$$X_{k-1} = [\lambda_{k-1} \quad \varphi_{k-1} \quad \lambda_k \quad \varphi_k \quad \cdots$$

$$\lambda_{k+8} \varphi_{k+8} V_{\lambda_{k+8}} V_{\varphi_{k+8}} a_{\lambda_{k+8}} \quad a_{\varphi_{k+8}}]^T_{24\times 1}$$

In the state vector, $[\lambda_{k-1} \quad \varphi_{k-1} \quad \lambda_k \quad \varphi_k \quad \cdots \lambda_{k+8}\varphi_{k+8}]$ are the positions of ten consecutive points in the navigation path and $[V_{\lambda_{k+8}} \quad V_{\varphi_{k+8}} \quad a_{\lambda_{k+8}} \quad a_{\lambda_{k+8}}]$ are the velocities and accelerations of the last waypoint in the point sequence.

The state vector updates one point each time; thus, the state transition matrix $\Phi_{k|k-1}$ can be established as follows:

$$\Phi_{k|k-1} = \begin{bmatrix} A_{18\times 20} & 0_{18\times 4} \\ & B_{6\times 6} \end{bmatrix}_{24\times 24}$$

The concrete form of matrix $A_{18\times 20}$, $B_{6\times 6}$ can be shown as

$$A_{18\times 20} = \begin{bmatrix} 0 & 0 & 1 & 0 & \cdots & 0 & 0 & 0 & 0 \\ & & 0 & 1 & 0 & \cdots & 0 & 0 & 0 \\ & & & 0 & 1 & 0 & \cdots & 0 & 0 \\ & & & & 0 & 1 & 0 & \cdots & 0 \\ & & & & & \ddots & \ddots & & \vdots \\ & & & & & & 0 & 1 & 0 \\ & & & & & & & 0 & 1 \end{bmatrix}_{18\times 20},$$

$$B_{6\times 6} = \begin{bmatrix} 1 & 0 & T & 0 & T^2/2 & 0 \\ 0 & 1 & 0 & T & 0 & T^2/2 \\ 0 & 0 & 1 & 0 & T & 0 \\ 0 & 0 & 0 & 1 & 0 & T \\ 0 & 0 & 0 & 0 & 1 & 0 \\ 0 & 0 & 0 & 0 & 0 & 1 \end{bmatrix}_{6\times 6}$$

The system noise matrix w_{k+1} can be shown as follows:

$$w_{k-1} = [w_{x_{k-1}} \quad w_{y_{k-1}} \quad w_{x_k} \quad w_{y_k} \quad \cdots$$
$$w_{x_{k+8}} w_{y_{k+8}} w_{vx_{k+8}} w_{vy_{k+8}} w_{ax_{k+8}} w_{ay_{k+8}}]^T_{24\times 1}$$

(2) The Establishment of the Observation Equation of CSITAN + WRIT

Since the derivation process has the same principle as that of traditional SITAN, here, we deliver the observation equation directly:

$$Z_k = H_k X_k + V(k) \tag{11}$$

In formula (11), $V(k) = \sum_{i=1}^{n} \gamma(i)_m - \sum_{i=1}^{n} \gamma_r(i) - \sum_{i=1}^{n} \gamma_l(i)$ represents the error terms, which contain the noises of measurement and quantization in the process of digital map making, the measurement noises, and the linearization errors.

The coefficient matrix is shown as follows:

$$H_k = [-h_\lambda(k), -h_\varphi(k), -h_\lambda(k+1), -h_\varphi(k+1), \cdots,$$
$$-h_\lambda(k+9), -h_\varphi(k+9), -h_\lambda(k+8)\cdot T,$$
$$-h_\varphi(k+8)\cdot T, \frac{-h_\lambda(k+8)T^2}{2}, \frac{-h_\varphi(k+8)\cdot T^2}{2}]_{1\times 24}$$

The last four terms in this coefficient matrix have the same meaning as that described in the traditional SITAN algorithm.

The Correlation Method

In this paper, we take the Mean Square Difference (MSD) algorithm, which is typically used in the Terrain Contour Matching (TERCOM) system as the decision method to find the most appropriate match result [22, 23].

The calculation formula of MSD algorithm is shown below:

$$J_{MSD}(\Delta e, \Delta n) = \frac{1}{n}\sum_{i=1}^{n}[g_r(i) - g_m(i)]^2 \qquad (12)$$

In formula (12), $g_r(i)$ represents the actual measurements of the gravity anomalies, $g_m(i)$ represents the extracted values of the gravity anomaly map corresponding to the predicted values $X_{k+1|k}$, n is the length of the point sequence, and Δe and Δn are the deviations in the direction of east and north, respectively. Under the condition that J_{MSD} gets the minimum value, we can obtain the best matched positions in a certain range of area [24, 25].

The Weight-Reducing Iteration Technique

In the course from X_k to X_{k+n-1}, the position parameters λ_{k+n-1} and φ_{k+n-1} have appeared for $n-1$ times at most (n is the length of the point sequence in the process of filtering), and the process is shown in Figure 4.

From Figure 4, we can see that the position of this waypoint λ_{k+n-1} and φ_{k+n-1} has been matched $n-1$ times. This can provide us with some statistical information, and thus, we can utilize the weight-reducing iteration technique to extract a value with higher precision [26, 27].

The principle of the weight-reducing iteration technique is shown in Figure 5:

P_i (k) and S_i (k) represent the weight and its variation coefficient of the i-th observation in the k-th time of adjustment. Δ represents the differences between the calculations of two adjacent adjustments, and τ is the threshold value. In the above process, $S_i(k) = V_{mean}(k)^2/V_i(k)^2$ and $V_{mean}(k)^2$ is the average value of $V_i(k)^2$ (i = 1,2 ...n). The weight of observations constantly change in the course of iteration, and observations with larger deviations get smaller variation coefficients. This will gradually raise the effects of observations with relatively higher accuracy. Results can be obtained through the adjustment at each time, except the last one if the differences between the results of two adjacent

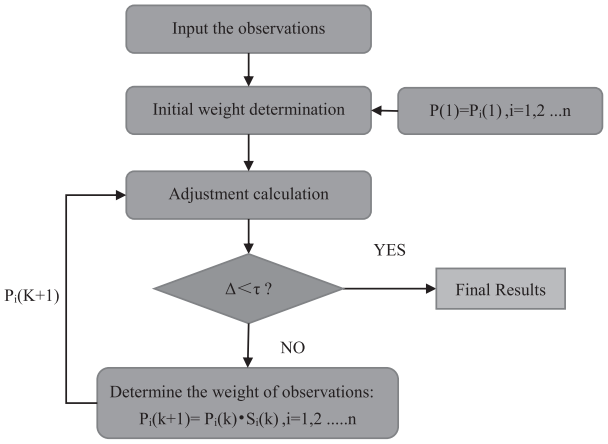

Fig. 5–The flow chart of weight-reducing iteration technique. [Color figure can be viewed at wileyonlinelibrary.com and www.ion.org]

adjustments are less than the threshold or the time of iteration exceeds the required number of times. The threshold value is selected based on the precision required in the navigation process, and we select 0.12 nmi as the threshold in this paper, which is equal to the random error of the positions assigned by INS.

EXPERIMENTS

Three different trajectories with gravity anomaly roughness values are selected to verify the feasibility and robustness of CSITAN + WRIT. The gravity anomaly data utilized in this paper were downloaded from the website of University of San Diego, who owns the spatial resolution of 1′ × 1′ (mGal as unit), [28].

Experimental Conditions

We set the same experimental conditions for both the traditional SITAN algorithm and CSITAN + WRIT, and the same INS information was utilized for the construction of the state transition matrix [29–31]. Figures 6–8 show the roughness distributions of the real trajectories in each case.

$$X_k = \left[\lambda_k \quad \varphi_k \quad \lambda_{k+1} \quad \varphi_{k+1} \quad \cdots \quad \lambda_{k+n-1} \quad \varphi_{k+n-1} \quad V_{\lambda_{k+n-1}} \quad V_{\varphi_{k+n-1}} \quad a_{\lambda_{k+n-1}} \quad a_{\varphi_{k+n-1}}\right]$$

$$X_{k+1} = \left[\lambda_{k+1} \quad \varphi_{k+1} \quad \lambda_{k+2} \quad \varphi_{k+2} \quad \cdots \quad \lambda_{k+n} \quad \varphi_{k+n} \quad V_{\lambda_{k+n}} \quad V_{\varphi_{k+n}} \quad a_{\lambda_{k+n}} \quad a_{\varphi_{k+n}}\right]$$

$$\cdots\cdots$$

$$X_{k+n-1} = \left[\lambda_{k+n-1} \quad \varphi_{k+n-1} \quad \lambda_{k+n} \quad \varphi_{k+n} \quad \cdots \quad \lambda_{k+2(n-1)} \quad \varphi_{k+2(n-1)} \quad V_{\lambda_{k+2(n-1)}} \quad V_{\varphi_{k+2(n-1)}} \quad a_{\lambda_{k+2(n-1)}} \quad a_{\varphi_{k+2(n-1)}}\right]$$

Fig. 4–Recursive example of point sequence in CSTIAN

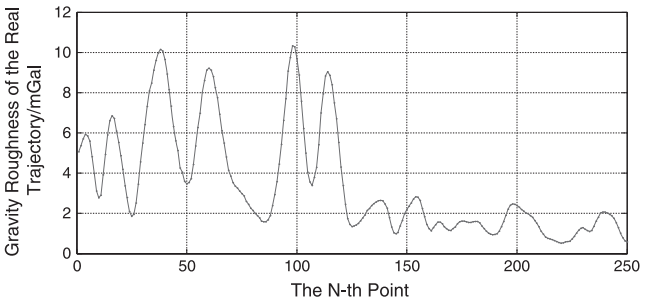

Fig. 6–The roughness values of the gravity anomaly of real trajectory in Experiment One. [Color figure can be viewed at wileyonlinelibrary.com and www.ion.org]

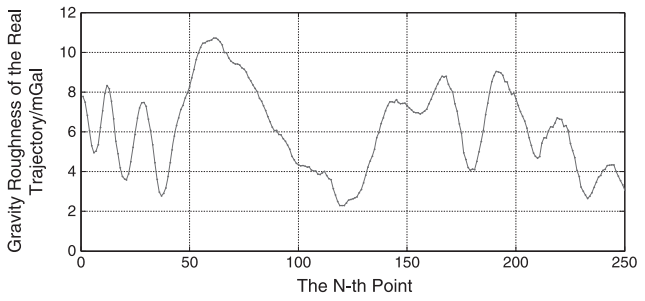

Fig. 7–The roughness values of the gravity anomaly of the real trajectory in Experiment Two. [Color figure can be viewed at wileyonlinelibrary.com and www.ion.org]

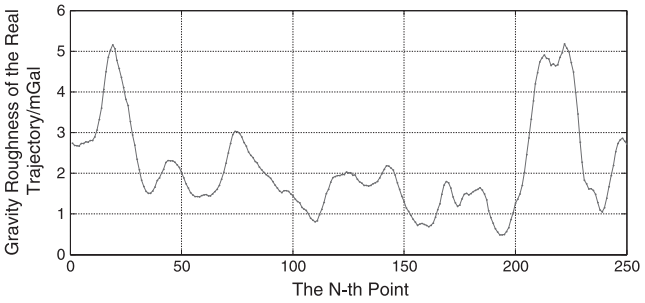

Fig. 8–The roughness values of the gravity anomaly of the real trajectory in Experiment Three. [Color figure can be viewed at wileyonlinelibrary.com and www.ion.org]

Figure 6 shows the roughness values of the gravity anomaly corresponding to the waypoints of the real trajectory in Experiment One. It is obvious that the roughness of the gravity anomaly in the first half of this trajectory is greater than that in the second half.

Figure 7 shows the roughness values of the gravity anomaly corresponding to the waypoints of the real trajectory in Experiment Two. The roughness of the gravity anomaly illustrated in this figure shows that it has relatively large values in almost the whole process.

Figure 8 shows the roughness values of the gravity anomaly corresponding to the waypoints of the real trajectory in Experiment Three. The roughness of gravity anomaly illustrated in this figure shows that it has relatively small values in almost the whole process when compared with the above two experiments.

More precise statistics of the roughness and simulation conditions of the three experiments are shown in Table 1.

In Table 1, L and B represent the direction of longitude and latitude respectively, and a negative value of speed means heading towards the opposite directions from east and north. The movement modes of the vehicles were simplified into linear motion in the experiments, and (0.12 + 0.06) nmi in the term of random error means that the INS assigned trajectories and the real trajectories have 0.12 nmi and 0.06 nmi of random errors, respectively. The trajectories in Experiment Two have relatively larger linear errors in the direction of latitude since it has larger roughness along its path.

Experimental Results

Experiment One

(1) Experimental Result of Traditional SITAN Algorithm

Figure 9 shows the matching effect and bias between matched trajectory (blue), real trajectory (black), and INS trajectory (red) when initial bias is $\delta B = \delta L = 1'$ (about 1 nmi). ΔL and ΔB represent the position bias in the direction of longitude and latitude. Figure 9(a) shows the matching effect, and 9(b) shows the position bias between the real trajectory and matched trajectory. The matched trajectory (blue) portrayed in (a) is relatively close to the real trajectory in the whole process but the occurrence of large matching errors of positions showed the instability of traditional SITAN.

(2) Experimental Result of CSITAN + WRIT

Figure 10 shows the matching effect and the bias between matched trajectory (blue), real trajectory (black), and INS trajectory (red) when initial bias is $\delta B = \delta L = 1'$ (about 1 nmi). ΔL and ΔB represent the position bias in the direction of longitude and latitude. Figure 10(a) shows the matching effect, and 10(b) shows the position bias between the real trajectory and matched trajectory. The matched trajectory (blue) portrayed in (a) is quite close to the real trajectory in the whole process. Without considering the initial waypoint of this trajectory, the bias in both directions, which is illustrated in (b), shows that the error was less than 0.5 nmi in the majority of this process and without the occurrence of divergence, which indicates that the matching process is rather successful.

Table 1—Statistics of the roughness and simulation conditions of the three experiments

		Experimental One	Experimental Two	Experimental Three
Roughness Value of Trajectory	Minimum	0.5249	2.2928	0.4887
	Maximum	10.3339	10.7228	5.1826
	Mean	3.4689	6.1436	2.1403
Sampling Interval	/	3 min	3 min	3 min
Number of Waypoints	/	250	250	250
Initial Position	L	131.2083°E	133.425°E	130.625°E
	B	27.6808°N	25.0379°N	27.8873°N
Initial Position Error	L	1 nmi	1 nmi	1 nmi
	B	1 nmi	1 nmi	1 nmi
Speed	L	12 nmi/h	−12 nmi/h	12 nmi/h
	B	10 nmi/h	6 nmi/h	−10 nmi/h
Linear Error	L	4 nmi/h	4 nmi/h	4 nmi/h
	B	1/6 nmi/h	1 nmi/h	1/6 nmi/h
Random Error	L	(0.12 + 0.06) nmi	(0.12 + 0.06) nmi	(0.12 + 0.06) nmi
	B	(0.12 + 0.06) nmi	(0.12 + 0.06) nmi	(0.12 + 0.06) nmi
Error of Gravity Measurements	/	1 mGal/2 mGal/ 3 mGal/4 mGal/ 5 mGal/6 mGal	1 mGal/2 mGal/ 3 mGal/4 mGal/ 5 mGal/6 mGal	1 mGal/ 2 mGal/ 3 mGal

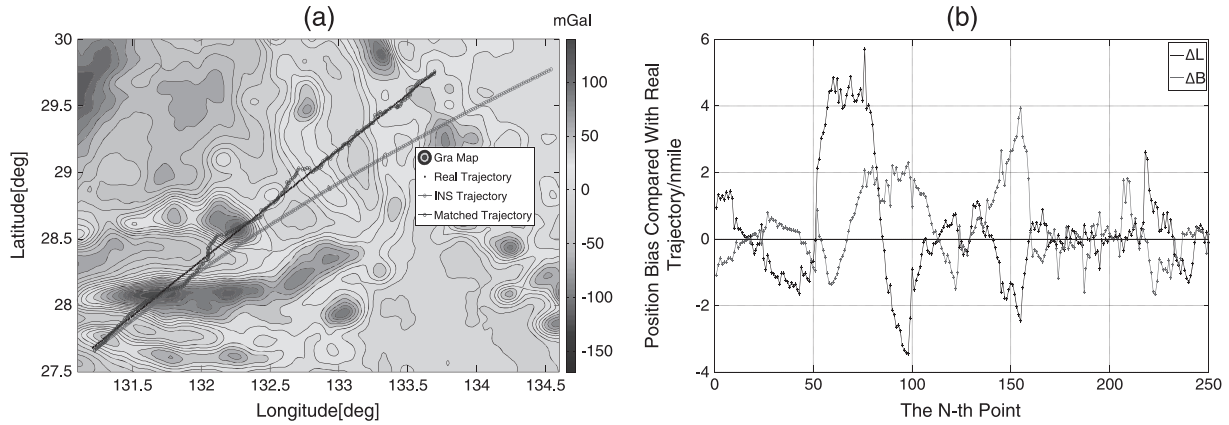

Fig. 9–Matching results of traditional SITAN algorithm. [Color figure can be viewed at wileyonlinelibrary.com and www.ion.org]

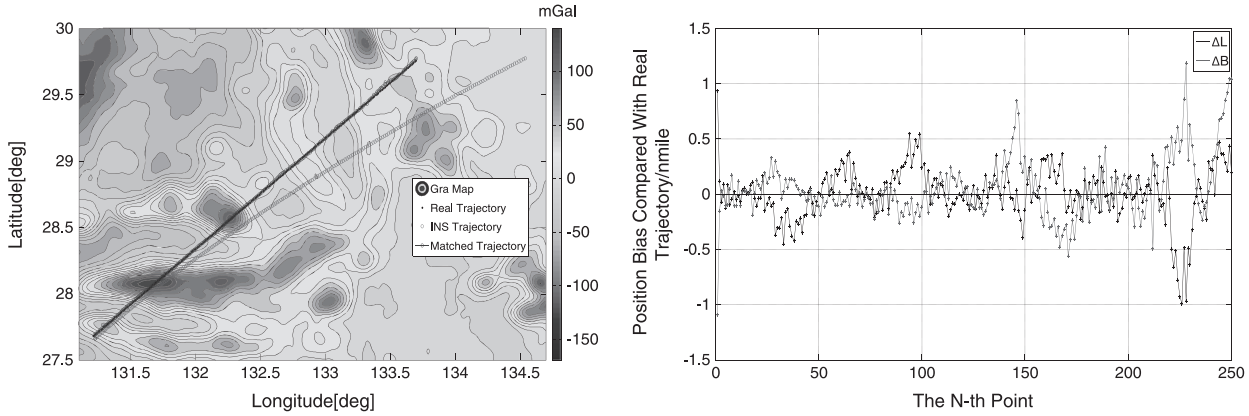

Fig. 10–Matching results of CSITAN + WRIT. [Color figure can be viewed at wileyonlinelibrary.com and www.ion.org]

Experiment Two

(1) Experimental Result of Traditional SITAN Algorithm

Figure 11 shows the matching effect and bias between matched trajectory (blue), real trajectory (black), and INS trajectory (red) of the underwater vehicle when the initial bias is $\delta B = \delta L = 1'$ (about 1 nmi). ΔL and ΔB represent the position bias in the direction of longitude and latitude. Figure 11(a) shows the matching effect, and 11(b) shows the position bias between the real trajectory and matched trajectory. The matched trajectory (blue) portrayed in (a) is close to the real trajectory in the

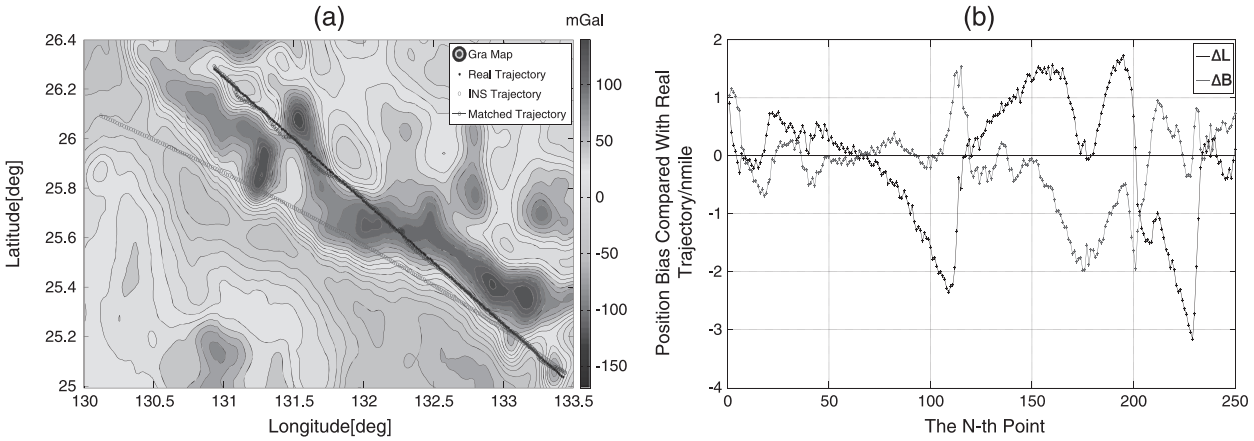

Fig. 11–Matching results of traditional SITAN algorithm. [Color figure can be viewed at wileyonlinelibrary.com and www.ion.org]

first half of this process. Without considering the initial waypoint of this trajectory, the bias in both directions, which is illustrated in (b), shows that the error was less than 2 nmi in the vast majority of this process and without the occurrence of divergence. The result indicates that the matching is successful.

(2) Experimental Result of CSITAN + WRIT

Figure 12 shows the matching effect and comparison between matched trajectory (blue), real trajectory (black), and INS trajectory (red) of the underwater vehicle when initial bias is $\delta B = \delta L = 1'$ (about 1 nmi). ΔL and ΔB represent the position bias in the direction of longitude and latitude. Figure 12 (a) shows the matching effect, and 12(b) shows the position bias between the real trajectory and matched trajectory. The matched trajectory (blue) portrayed in (a) is quite close to the real trajectory in the whole process. Without considering the initial waypoint of this trajectory, the bias in both directions, which is illustrated in (b), shows that the error was less than 0.5 nmi in the vast majority of this process and without the occurrence of divergence. The maximal value of the bias barely reaches 1.5 nmi and 1 nmi in the direction of longitude and latitude, which is much smaller than that occurring in the traditional SITAN algorithm. The result indicates that the matching is successful.

Experiment Three

(1) Experimental Results of Traditional SITAN Algorithm

Figure 13 shows the matching effect and bias between matched trajectory (blue), real trajectory (black), and INS trajectory (red) of the underwater vehicle when initial bias is $\delta B = \delta L = 1'$ (about 1 nmi). ΔL and ΔB represent the position bias in the direction of longitude and latitude. Figure 13(a) shows the matching effect, and 13(b) shows the position bias between the real trajectory and matched trajectory. Due to the relatively small roughness values of the gravity anomaly and the accumulation of INS errors, divergence occurred around the 100th point (Figure 8 shows that there is also a decline of the roughness values of the gravity anomaly before the 100th point). The matched trajectory (blue) portrayed in (a) and the

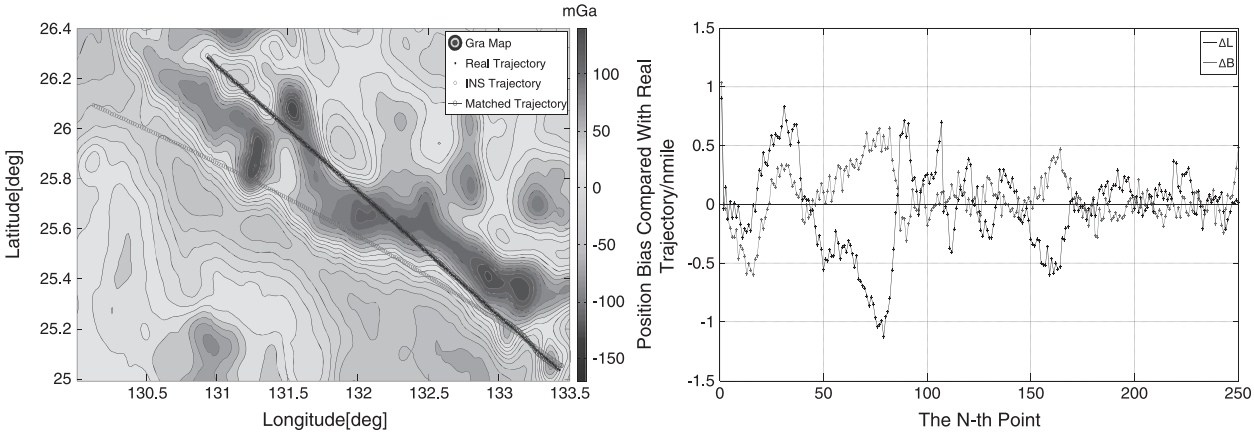

Fig. 12–Matching results of CSITAN + WRIT. [Color figure can be viewed at wileyonlinelibrary.com and www.ion.org]

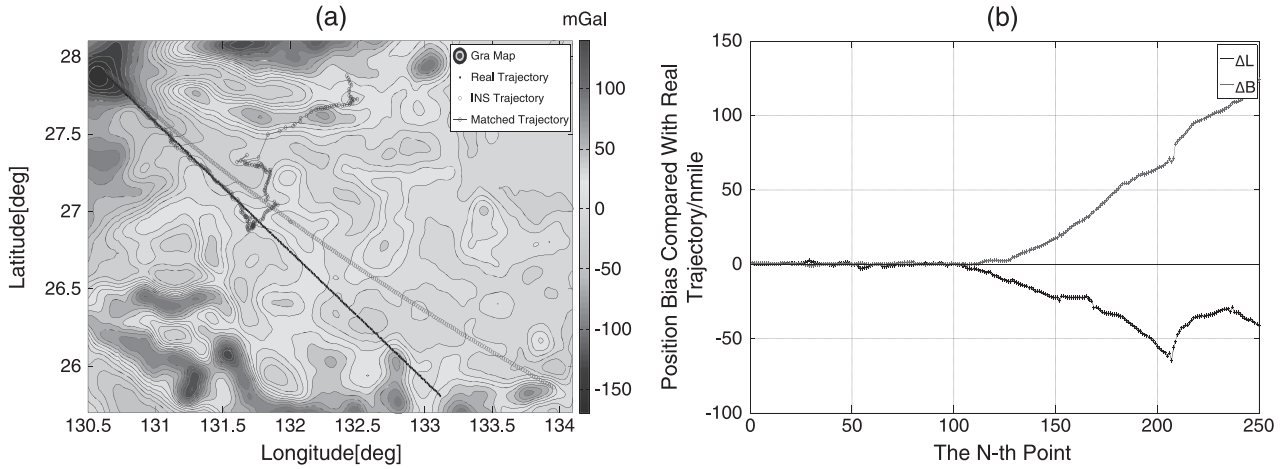

Fig. 13–Matching results of traditional SITAN algorithm. [Color figure can be viewed at wileyonlinelibrary.com and www.ion.org]

bias illustrated in (b) show that the matching process is unsuccessful.

(2) Experimental Results of CSITAN + WRIT

Figure 14 shows the matching effect and bias between matched trajectory (blue), real trajectory (black), and INS trajectory (red) of the underwater vehicle when initial bias is $\delta B = \delta L = 1'$ (about 1 nmi). ΔL and ΔB represent the positions bias in the direction of longitude and latitude. Figure 14(a) shows the matching effect, and 14(b) shows the position bias between the real trajectory and matched trajectory. The matched trajectory (blue) portrayed in (a) and the bias illustrated in (b) show that the matching process is rather successful.

Analysis of the Experimental Results

In this section, we give the statistics of the experimental results to verify the feasibility and robustness of the improved CSITAN + WRIT algorithm, which include the convergence conditions and the root mean square error of matched positions $\Delta S_i^1, \Delta S_i^2$ of the traditional SITAN algorithm and CSITAN + WRIT, respectively. Table 2 shows the statistics of the experimental results in the above three experiments.

The number of waypoints is 250 in each experiment, and the length of the point sequence is 10. The number of convergence points does not include the first ten in the trajectory for it takes time to converge. Thus, 240 convergence points means without the occurrence of divergence while * in Table 2 means that the number of convergence points is less than 30. This table shows four things: (1) Traditional SITAN and CSITAN + WRIT both achieved better matching results in Experiment One and Experiment Two when compared with the results in Experiment Three, proving that larger roughness values of gravity anomalies bring better matching results. (2) Traditional SITAN diverges when the error of the gravity measurement is larger than 1 mGal in Experiment One and 2 mGal in Experiment Two with relatively larger roughness values of gravity anomalies. CSITAN + WRIT converged and achieved 2.3647 nmi and 2.9709 nmi of positional accuracy when the error of gravity measurement was 5 mGal in the first two experiments. In Experiment Three with small roughness values for gravity anomalies, even the

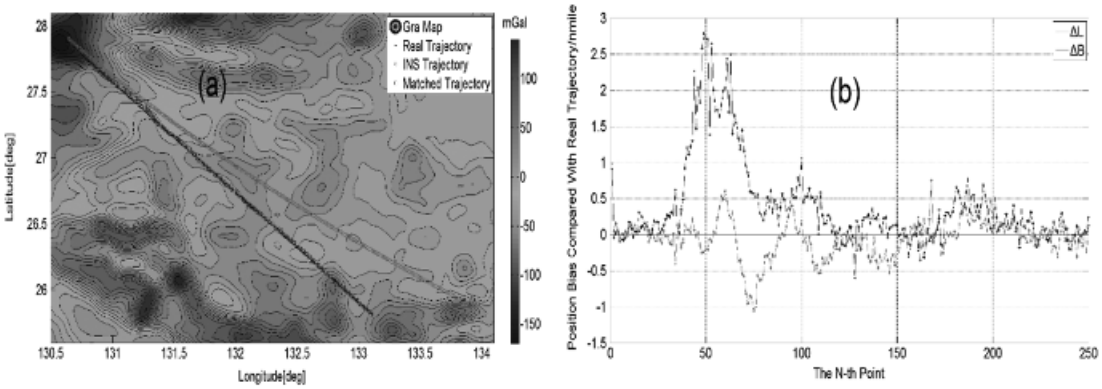

Fig. 14–Matching results of CSITAN + WRIT. [Color figure can be viewed at wileyonlinelibrary.com and www.ion.org]

Table 2—Statistics of the experimental results

	Mean Roughness Value	Error of Gravity Measurement (mGal)	Traditional SITAN		CSITAN + WRIT	
			Number of Convergence Point	RMS of Position Bias (nmi)	Number of Convergence Point	RMS of Position Bias (nmi)
Experiment One	3.4689	1	240	2.0539	240	0.3635
		2	65	4.3653	240	0.7048
		3	50	5.3320	240	1.2960
		4	40	5.8424	240	1.8309
		5	*	*	240	2.3647
		6	*	*	190	4.9266
Experiment Two	6.1436	1	240	1.2977	240	0.4312
		2	240	3.8638	240	0.9489
		3	140	2.8344	240	1.6783
		4	90	2.3993	240	2.8109
		5	90	2.9072	240	2.9709
		6	70	3.9368	190	3.3204
Experiment Three	2.1403	1	100	1.1941	240	0.7960
		2	95	2.0552	160	1.2403
		3	80	4.4854	150	2.9383

CSITAN + WRIT diverged when the error of gravity measurement is larger than 1 mGal with 0.7960 nmi of positional accuracy. (3) CSITAN + WRIT achieved better positional accuracy than traditional SITAN even when converged. (4) With the increase of the error of gravity measurement, the positional accuracy declined. The results of Experiment One are slightly better than those in Experiment Two because the linear error in the direction of latitude in Experiment Two is relatively larger than that in Experiment One.

The experimental results indicated that CSITAN + WRIT improved the accuracy in areas where the roughness values of the gravity anomaly are relatively large and the robustness in areas where the roughness values of the gravity anomaly are relatively small.

CONCLUSION AND DISCUSSION

The experimental results validated the improvement of feasibility and robustness of SITAN. The main scientific results from the experiments are summarized below:

(1) CSITAN + WRIT can achieve better accuracy in areas where the roughness values of the gravity anomaly are relatively large and increase the success rate of matching in areas where the roughness values of the gravity anomaly are relatively small.
(2) A suitable matching area needs to be selected for both traditional SITAN and CSITAN + WRIT before setting sail because the characteristics of the gravity field have a great influence on matching results.

It is important to note that even with improvements from CSITAN + WRIT, there is still some work that needs to be done:

(1) Different numbers of waypoints in the recursive sequence need to be tested in order to find out the optimal length of the recursive sequence.
(2) Carry out experiments under different error conditions to find out the rule between the INS errors and the matching results, thus confirming the maximum tolerance of different errors.

ACKNOWLEDGMENT

This research is funded by the National Natural Science Foundation of China (grant no. 41374012).

REFERENCES

1. Li, S. S., *Research on the Theory and Method of Underwater Gravity-Aided Inertial Navigation Systems*, Dissertation for the degree of D. Eng., Zheng Zhou, PLA Information Engineering University, 2010.
2. Kamgar-Parsi, B., "Vehicle Localization on Gravity Maps," *Proceedings of SPIE – The International Society for Optical Engineering*, 1999, p. 3693.
3. Kim, J. and Sukkarieh, S., "Autonomous Airborne Navigation in Unknown Terrain Environments," *IEEE Transactions on Aerospace and Electronics Systems*, Vol. 40, No. 3, 2004, pp. 1031-1045.
4. Jircitano, A. and Dosch, D. E., "Gravity Aided Inertial Navigation System (GAINS)," *Proceedings of the 47th Annual Meeting of The Institute of Navigation*, Williamsburg, VA, June 1991, pp. 221–229.
5. Javed, W., Ghani, S., and Elmqvist, N., "GravNav: Using a Gravity Model for Multi-Scale Navigation," *The Workshop on Advanced Visual Interfaces (AVI)*, 2012, pp. 217–224.
6. Wang, T., *Study on Arithmetic and Application of Sandia Inertial Terrain-Aided Navigation*, Dissertation, Northwestern Polytechnic University, 2006.

7. Boozer, D. D. et al., "AFTI/F16 Terrain-Aided Navigation System," *National Aerospace and Electronic Conference*, Dayton, OH, May 1985.
8. Hollowell, J., "Heli/SITAN: A Terrain Referenced Navigation Algorithm for Helicopters," *Proceedings of the IEEE Position, Location, and Navigation Symposium (PLANS)*, Las Vegas, NV, 1990.
9. Yang, Z., Zhu, Z., and Zhao, W., "A Triangle Matching Algorithm for Gravity-Aided Navigation for Underwater Vehicles," *Journal of Navigation*, Vol. 67, No. 2, 2013, pp. 227-247.
10. Flament, M., Fleury, G., and Davoust, M. E., "Particle Filter and Gaussian-Mixture Filter Efficiency Evaluation for Terrain-Aided Navigation," *Proceedings of the IEEE European Signal Processing Conference*, 2004.
11. Metzger, J. et al., "Sigma-Point Filter for Terrain Referenced Navigation," 2000.
12. Nordlund, P. J. and Gustafsson, F., "Marginalized Particle Filter for Accurate and Reliable Terrain-Aided Navigation," *IEEE Transactions on Aerospace and Electronics Systems*, Vol. 45, No. 4, 2009, pp. 1385-1399.
13. Yoo, Y. M. et al., "Improvement of TERCOM-Aided Inertial Navigation System by Velocity Correction," *Proceedings of IEEE/ION Position, Location and Navigation Symposium (PLANS)*, Myrtle Beach, South Carolina, April 2012, pp. 1082–1087.
14. Fanming, et al., "Application of Kalman Filter Algorithm in Gravity-Aided Navigation System," *Proceedings of the IEEE 2011 International Conference on Mechatronics and Automation (ICMA)*, 2011, pp. 2322–2326.
15. Welch, G. and Bishop, G., "An Introduction to the Kalman Filter," University of North Carolina at Chapel Hill, Vol. 7, 1995, pp. 127–132.
16. Zheng, T., Wang, Z. G., and Bian, S. F., "Improvement on SITAN Algorithm for Seabed Terrain-Aided Navigation," *Ship Electric Engineering*, Vol. 28, No. 7, 2008, pp. 69–71.
17. Chai, L. and Fang, Q., "Different Selection of Measurements in SITAN Terrain Auxiliary Navigation System", *Journal of Projectiles, Rockets, Missiles and Guidance*, Vol. 22, No. 3, 2002, pp. 78-80.
18. Xu, D. X., Wang, Y., Wang, H. B., Cai, X. B., and Dai, Q. F., "Result Analysis of Vertical Gradient of Gravity and Gravity Anomaly Aided Navigation with SITAN Algorithm," *Journal of Geodesy and Geomatics*, Vol. 31, No. 1, 2011, pp. 127-131.
19. Dai, Z. G. and Kang, C., "Geomagnetic Field-Aided Inertial Navigation Using the SITAN Algorithm," *2nd International Conference on Systems and Informatics (CSAI)*, 2014, pp. 79–83.
20. Sun, Y., Wang, S. C., Qiao, Y. K., Zhang, J. S., Sun, D. W., and Wang, X. B., "Research on SITAN in Geomagnetic-Aided Inertial Navigation System," 2009 *National Symposium on National Security and Geophysics*, 2009.
21. Wu, L., Ma, J., and Tian, J., "A Self-Adaptive Unscented Kalman Filtering for Underwater Gravity Aided Navigation," *Proceedings of the IEEE/ION Position, Location, and Navigation Symposium (PLANS)*, Indian Wells, California, May 2010, pp. 142–145.
22. Li, X. W., Liu, J. Y., and Kang, G. H., "Development and Application of TERCOM Elevation-Aided Navigation System," *Journal of Chinese Inertial Technology*, Vol. 14, No. 1, 2006, pp. 34-40.
23. Baker, B. W. and Clem, R., "Terrain Contour Matching (TERCOM)," *Primer*, ASD-TR77-61, Aeronautical Systems Division, Wright-Patterson AFB, 2010.
24. Wiener, T. F., "Terrain Contour Matching (TERCOM): A Cruise Missile Guidance Aid," *Technical Symposium*, 1980, pp. 10–18.
25. Tong, Y. D., Bian, S. F., and Ji, B., "Real-Time Maximum Correlation Matching Based on Approximated Local Gravity Map," *China Satellite Navigation Academic Annual Conference*, 2012, pp. 493–503.
26. Yang, J. and Tao, Y. Q., "Total Least Squares Algorithm for Coordinate Conversion," *Science of Surveying and Mapping*, Vol. 40, 2015, pp. 15-18.
27. Wu, Z. H., Luo, W. Z., and Li, J., "On Position of Gross Errors of Common Points in Coordinate Transformation and Reducing Influence of Gross Errors," *Journal of Geodesy and Geomatics*, Vol. 34, No. 1, 2014, pp. 118-122.
28. Satellite Geodesy at the Scripps Institution of Oceanography, University of California San Diego (EB/OL), 2014, http://topex.ucds.edu/.
29. Yan, L., "Research on the Selection of Suitable Matching Area in the Gravity Aided Navigation," Geoinformatics, 2007 International Society for Optics and Photonics, 2007:67523U-67523U-12.
30. Yan, L., Cui, C., and Wu, H., "A Gravity Matching Algorithm Based on TERCOM, *Geomatics and Information Science of Wuhan University*, Vol. 3, pp. 261–264.
31. Xiong, H. et al., "Research on the Algorithm of Gravity Aided Inertial Navigation Based on CKF," 2014, pp. 252–257.